Pergamon

Int. J. Heat Mass Transfer. Vol. 39, No. 4, pp. 725–733, 1996

0017-9310/96 $15.00 + 0.00

0017-9310(95)00179-4

Enhancement of energy charge–discharge rates in composite slabs of different phase change materials

ZHEN-XIANG GONG and ARUN S. MUJUMDAR
Department of Chemical Engineering, McGill University, Montreal, Canada H3A 2A7

(*Received* 30 *August* 1994 *and in final form* 8 *May* 1995)

Abstract—A one-dimensional finite element phase change heat conduction model has been developed for cyclic melting–freezing in composite phase change material (PCM) slabs. Computations have been carried out to investigate the influence of different arrangements of PCMs with different melting points, thermophysical properties and different boundary conditions on the transient heat transfer process when energy is charged from one side of a slab and discharged from the other. Numerical experiments indicate that the instantaneous heat flux can be greatly enhanced using slabs consisting of multiple composite PCMs. Potential for application of composite PCMs in thermal energy storage is discussed.

INTRODUCTION

Latent heat thermal storage has proved to be an effective way for solar energy utilization and industrial waste heat recovery due to its high storage density and small temperature variation from storage to retrieval. In a latent heat storage system, energy is stored during melting and recovered during freezing of the PCMs. Prediction of such alternating melting–freezing heat transfer processes is the key to optimal design of the energy storage system. Despite the significance of the alternative melting–freezing processes, research work on such problems has received little attention so far.

Bransier [1] appears to have been the first to analyze cyclic melting–freezing of a phase change material. He used a one-dimensional (1D) conduction model to analyze a slab and a concentric module and found that a maximum of two interfaces could coexist during cyclic melting–freezing. Kalhori and Ramadhyani [2] carried out a cyclic melting–freezing experiment with unfinned and finned vertical cylinders embedded in a 99% pure *n*-ecosane and observed multiple layers of solid and liquid during the initial periods consisting of the first three and four cycles. Jariwala *et al.* [3] studied experimentally the cyclic thermal performance of a latent heat storage unit which consisted of a cylindrical helically coiled copper tube embedded in a cylindrical tank of a commercial paraffin wax. The predictions of a quasi-steady 1D model developed were found to match well with the experimentally measured periodic energy stored or recovered. Hasan [4] developed a 1D cyclic phase change heat conduction model for a plane slab and carried out a detailed parametric study about the effects of various parameters on the energy charge–discharge. He also carried out experiments on alternate melting–freezing of *n*-octadecane in a thin rectangular cell and found the numerical results to be in good agreement with his experimental data. Sasaguchi and Viskanta [5] investigated experimentally the effects of free convection on the melting and resolidification of 99.9% pure *n*-octadencane around two cylindrical pipes spaced vertically. Adebiyi [6] carried out a second-law analysis for packed bed cyclic storage systems utilizing phase-change materials. Bellecci and Conti [7–9] set up a numerical model to simulate the cyclic behaviour of the latent heat thermal storage system in a solar receiver unit. Using their model they developed criteria for optimal design of such storage systems. Kerslake and Ibrahim [10] also reported an alternative melting–freezing simulation of the thermal storage system in the proposed space station "Freedom".

As for the research of cyclic melting–freezing heat transfer in composite PCMs, Gong *et al.* [11] seem to have been the first authors to analyze alternative melting–freezing processes in composite PCM slabs. They developed a 1D finite element conduction model to simulate cyclic melting–freezing and found the instantaneous heat flux on the heat transfer surface could be enhanced in a binary composite PCM slab during the cyclic melting–freezing processes at the steady reproducible state (SRS) when energy is charged and discharged from the same side of the slab. Gong and Mujumdar [12] further investigated the effects of different arrangements of PCMs with different melting points on the charge–discharge rates of thermal energy in the cyclic melting–freezing in composite slabs of multiple PCMs when energy is charged and discharged also from the same side.

Farid *et al.* [13, 14] proposed a thermal energy storage system using multiple families of PCMs which were contained in a number of cylindrical capsules with air flowing across them. Lim *et al.* [15] carried

NOMENCLATURE

c	specific heat
ΔH	enthalpy change
$[C]$	heat capacity matrix
f_H	enthalpy–temperature function
f_T	temperature–enthalpy function
f_{iH}	enthalpy–temperature function of PCM i
f_{iT}	temperature–enthalpy function of PCM i
$\{F\}$	heat load vector
k	heat conductivity
$[K]$	conductance matrix
h	enthalpy of unit mass
L	thickness of a PCM slab
L_i	thickness of PCM i
m	number of PCMs in a slab
$[M]$	lumped mass matrix
n	number of cycle
N_I, N_J	shape function
Q	instantaneous energy charged or discharged
Q_M	maximum possible energy charged or discharged in a period
Q_T	energy charged or discharged in a period
t	time
Δt	time step
t_f	freezing time
t_m	melting time
t_p	$= t_m + t_f$
T	temperature
T_0	initial temperature
T_{mi}	melting point of PCM i
T_w	boundary temperature
T_{wf}	boundary temperature during freezing
T_{wm}	boundary temperature during melting
x	co-ordinate.

Greek symbols

λ	latent heat
Ω^e	domain of an element
ρ	density.

Superscripts

e	estimated value
l	liquid
n	nth time step
s	solid.

Subscripts

cor	correction
i	PCM i
I,J	number of an element node.

out a second-law analysis on use of multiple PCMs placed in series and melted by the same stream of hot fluid. They noted the use of multiple PCMs could reduce the exergy loss of the system and obtained the optimal condition for systems composed of two or infinite number of PCMs. Adebiyi *et al.* [16] reported that the efficiency for the system utilizing five PCM families in a packed bed latent heat storage system exceeded that for the single PCM family by as much as 13–26%. Watanabe *et al.* [17] extended the experiments of ref. [14] using water as the heating and cooling medium and proved that there was enhancement of the charge–discharge rates in the latent heat storage system using three PCMs.

In this paper a 1D finite element phase change heat conduction model will be developed for alternating melting–freezing of a slab consisting of several different immiscible PCMs subjected to cyclical boundary conditions. The PCMs are separated by thermally thin barriers. Simulations will be carried out for single and composite PCM slabs to investigate the effects of different arrangements of the PCMs with different melting points and thermophysical properties and the effects of different boundary conditions on the charge–discharge rates of thermal energy when energy is charged from one side of a composite slab and discharged from the other.

MATHEMATICAL FORMULATION

The physical system considered is a thin slab composed of 'm' PCMs (Fig. 1). In each cycle thermal energy is charged from the upper face of the slab and discharged from the lower face. When heat is supplied from the upper face, the lower face keeps insulated; while as the heat is recovered from the lower face, the upper face is insulated. We assume the boundary is held at fixed temperatures, T_{wm} and T_{wf}, during the charge and discharge processes, respectively.

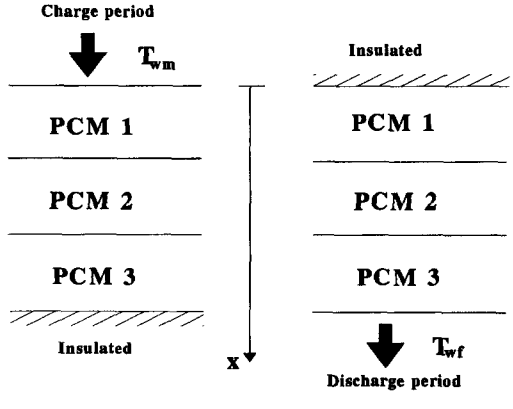

Fig. 1. Physical model.

For a mathematical description of the heat transfer process, the following assumptions are made: (1) the 'm' PCMs in the slab are immiscible and each is isotropic and homogenous; (2) heat transfer in each PCM is conduction-controlled; (3) the densities of the solid and liquid of each PCM are equal and (4) the thermal resistance at the interfaces of the PCMs is neglected. In future computations all of these restrictions will be eliminated.

Based on the above assumptions, the governing equations for the melting–freezing heat transfer processes are as follows:

for PCM $i (i = 1, 2, \ldots m)$,

Solid region:

$$\rho_i \frac{\partial h}{\partial t} = k_i^s \frac{\partial^2 T}{\partial x^2}. \tag{1}$$

Melt region:

$$\rho_i \frac{\partial h}{\partial t} = k_i^l \frac{\partial^2 T}{\partial x^2}. \tag{2}$$

The initial and boundary conditions are:

$$T(x, 0) = T_0 \quad \text{for} \quad 0 \leqslant x \leqslant L \tag{3}$$

$$T(0, t) = T_{wm}, \frac{\partial T(L, t)}{\partial x} = 0$$

$$\text{for} \quad nt_p < t \leqslant nt_p + t_m \tag{4}$$

$$T(L, t) = T_{wf}, \frac{\partial T(0, t)}{\partial x} = 0$$

$$\text{for} \quad nt_p + t_m < t \leqslant (n+1)t_p \tag{5}$$

where $n = 0, 1, 2, 3, \ldots$

FINITE ELEMENT MODEL

For convenience in future work in this area which will extend the model to 2D and 3D problems, an enthalpy-based equivalent heat capacity approach proposed by Pham [18] is employed to handle the phase change effects.

After the spacewise discretization of equations (1) and (2) using the standard Galerkin finite element method [19], we have the following semi-discrete equation:

$$[C]\{\dot{T}\} + [K]\{T\} = \{F\} \tag{6}$$

where the superposed dot denotes differentiation with respect to time; $[C]$ and $[K]$ are heat capacity and conductivity matrices, respectively, and typical elements in the matrices are:

$$C_{IJ} = \sum \int_{\Omega^e} \rho c N_I N_J \, dx \tag{7}$$

$$K_{IJ} = \sum \int_{\Omega^e} k \frac{\partial N_I}{\partial x} \frac{\partial N_J}{\partial x} dx. \tag{8}$$

In the above, summations are taken over the contributions of each element. For problems with the first kind of boundary condition (fixed temperature) as well as an insulated boundary condition, $\{F\}$ in equation (6) is equal to $\{0\}$. In this work two-point liner elements will be used to perform all computations.

A three time-level scheme [20] incorporating the lumped heat capacity [18] is used to accomplish the time discretization of equation (6). After time discretization, we obtain:

$$([C^*] + \tfrac{3}{4}\Delta t[K^*])\{T^{n+1}\} = [C^*]\{T^n\} - \tfrac{1}{4}\Delta t[K^*]\{T^{n-1}\} + \Delta t\{F^*\} \tag{9}$$

where the superscript * designates that the matrices and vectors are evaluated at $\{T^*\} = \{T^n\}$ or $\{T^*\} = \{1.5T^n - 0.5T^{n-1}\}$. The solution steps of equation (9) are as follows:

(1) *Calculation of the equivalent heat capacity*

At the beginning of each time step, the enthalpy change at each node is estimated from the known temperature field at time level n as follows:

$$\{\Delta H^e\} = [M^n]^{-1}(\{F^n\} - [K^n]\{T^n\})\Delta t. \tag{10}$$

The estimated new enthalpy field is

$$\{H^e\} = \{H^n\} + \{\Delta H^e\}. \tag{11}$$

Therefore, the estimated new temperature field is

$$\{T^e\} = \{f_T(H^e)\}. \tag{12}$$

The specific heat is then defined as

$$\{c^n\} = \{\Delta H/(T^e - T^n)\}. \tag{13}$$

(2) *Solution of the discrete matrix equation*

Calculate the lumped [C] using the value of $\{c^n\}$ from equation (13) and then solve equation (9) to obtain $\{T^{n+1}\}$.

(3) *Correction of the temperature*

The following correction step is applied to $\{T^{n+1}\}$,

$$\{T_{cor}^{n+1}\} = \{f_T(f_H(T^n) + c^n(T^{n+1} - T^n))\}. \tag{14}$$

It should be noted that equation (13) has no solution when $T^e = T^n$, i.e. when a step change in the enthalpy temperature curve is encountered. To overcome this problem, the step change in enthalpy is forced to take place over a finite but arbitrarily small width to prevent c^n in equation (13) from becoming infinite.

CHARGE AND DISCHARGE OF ENERGY

The instantaneous temperature distributions in the composite PCMs are obtained using the aforementioned numerical scheme. The magnitude of the cumulative energy charged or discharged per unit area, Q, is calculated as a function of time for each melting or freezing period. This calculation is made by computing the enthalpy of the PCMs at each time increment using the solid PCMs at their fusion tem-

peratures as the reference states and then subtracting the enthalpy of the PCMs at the beginning of the period. The value of Q is zero at the beginning of a period and it increases over a period toward Q_T, the cumulative energy charged or discharged in the period.

The maximum amount of energy which can be charged or discharged in a melting or freezing period is

$$Q_M = \sum_{i=1}^{m} \rho_i L_i [f_{iH}(T_{wm}) - f_{iH}(T_{wf})]. \quad (15)$$

A cycle consists of one melting and the following freezing period.

RESULTS AND DISCUSSION

To the authors' knowledge, no experimental results are available to validate the present cyclic melting–freezing in a composite slab of different phase change materials. However, the numerical model mentioned above was compared with analytical solutions for simple melting and freezing problems and found to be accurate and independent of mesh size. Also it was compared with experimental results of cyclic melting–freezing in a single-PCM slab [4] and the numerical results were found to be in good agreement with the experimental ones.

In order to investigate the effects of various parameters on energy charge–discharge rates in each cycle, melting and freezing processes in 2- and 3-PCM slabs are simulated.

Initially the composite slab is assumed to be at a uniform temperature of 26°C. At the start of the first cycle, the upper face of the slab (Fig. 1) is subjected to a constant temperature, T_{wm}, which is above the fusion temperatures of the PCMs, while the lower surface is adiabatic. In the following freezing period, the upper face of the slab is adiabatic, while the lower face is subjected to a constant temperature, T_{wf}, which is below the fusion temperatures of the PCMs. In the second and the following cycles these boundary conditions are repeated.

(1) *Effects of PCM melting points*

A single PCM slab was simulated using parameters listed in Table 1. Numerical experiments indicated that the cumulative energy charged–discharged in each cycle is within 1.41% different using 30 elements with a time step size of 0.25 s compared with 90 elements with a time step size of 0.025 s. Therefore, to speed up computations, all simulations use 30 elements with a time step of 0.25 s. Dynamic simulations are carried out until a steady reproducible state (SRS) is reached. In this state, the transient phase change heat transfer process occurs repeatedly from cycle to cycle and the cumulative energy charged–discharged in each melting or freezing period is the same.

Table 1. Parameters for single PCM slab

ρ	100 kg m^{-3}	T_m	90°C
k^s	1.0 W m^{-1} K^{-1}	L	0.1 m
k^l	1.0 W m^{-1} K^{-1}	T_{wm}	120°C
c^s	400 J kg^{-1} K^{-1}	T_{wf}	60°C
c^l	400 J kg^{-1} K^{-1}	t_m	600 s
λ	40 000 J kg^{-1}	t_f	600 s

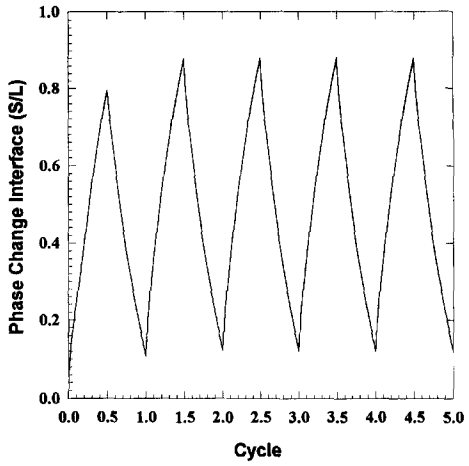

Fig. 2. Phase change interface movement vs time for single PCM slab.

Figure 2 displays the movement of the phase change interface with time. At the start of the first cycle, the upper face of the slab ($S/L = 0$) is subjected to a constant temperature of 120°C which is above the melting point of the PCM (90°C), while the lower face ($S/L = 1$) is insulated. With time the melting interface begins to progress from the upper face to the lower face. At the end of the melting period, i.e. at cycle = 0.5, the melting interface reaches $S/L \cong 0.8$. This indicates that in the first melting period, about 80% of the PCM is melted. Following the end of this melting period, the freezing period begins. In the freezing period, the upper face of the slab is insulated while the lower face is subjected to a constant temperature of 60°C which is below the melting point of the PCM. In this period, the melting interface shrinks toward the upper face ($S/L = 0$) and at the end of the freezing period, the melting interface reaches $S/L \cong 0.11$. At this moment, the first melting–freezing cycle is completed. Following the end of the first cycle the second melting period begins. The melting interface begins to extend from $S/L \cong 0.11$ toward the lower face. At the end of the this melting period, the melting interface reaches $S/L \cong 0.88$. When the second freezing period ends, the melt interface shrinks to the location of $S/L \cong 0.12$. In the third cycle, the alternative melting–freezing process reaches the SRS and in subsequent cycles, the interface movement is repeated indefinitely.

Following the computation for the single PCM slab, computations were carried out for 2-PCM and 3-PCM composite slabs. The boundary temperatures (T_{wm}

and T_{wf}), the total thickness of the slab, as well as the thermophysical properties except for the melting points of the PCMs which consist of the 2-PCM slabs or 3-PCM slabs were assumed to be all the same as those of the single PCM case. For the 2-PCM and 3-PCM slabs, $L_1 = L_2 = \frac{1}{2}L$ and $L_1 = L_2 = L_3 = \frac{1}{3}L$ are specified respectively. Tables 2 and 3 present the comparisons of the cumulative energy charged–discharged in each period at the SRS in different 2-PCM and 3-PCM slabs, respectively, with that in the single PCM slab.

From Table 2 we can see that different enhancements of the cumulative energy charged–discharged in each melting or freezing period at SRS can be obtained using different arrangements of the PCMs with different melting points when compared with the single PCM slab. The enhancement of the cumulative energy charged–discharged in case 3 (Table 2) is the highest, namely 15.2%. This means that the charge–discharge rates of thermal energy can be 15.2% faster using such a 2-PCM composite slab than the single PCM slab. From this case we note that the melting points of the two PCMs are decreased equally from the melting boundary temperature T_{wm} (storage temperature) to the freezing boundary temperature T_{wf} (retrieval temperature). This indicates that when the melting points of the two PCMs are selected to be equal in difference from the storage temperature to the retrieval temperature, the enhancement of the energy charge–discharge rates is maximum. Of course optimal melting point allocation is also determined by the thermophysical properties of the PCMs.

Table 2. Energy charge–discharge in 2-PCM slabs

Case	[°C]	Q_T [J m^{-2}]	Q_T/Q_M	Enhancement [%]
1	$T_{wm} = 120$ $T_m = 90$ $T_{wf} = 60$	404 508	0.632	—
2	$T_{wm} = 120$ $T_{m1} = 95$ $T_{m2} = 85$ $T_{wf} = 60$	448 730	0.701	10.9
3	$T_{wm} = 120$ $T_{m1} = 100$ $T_{m2} = 80$ $T_{wf} = 60$	466 157	0.728	15.2
4	$T_{wm} = 120$ $T_{m1} = 105$ $T_{m2} = 75$ $T_{wf} = 60$	463 964	0.725	14.7
5	$T_{wm} = 120$ $T_{m1} = 110$ $T_{m2} = 70$ $T_{wf} = 60$	423 391	0.66	4.67

Table 3. Energy charge–discharge in 3-PCM slabs

Case	[°C]	Q_T [J m^{-2}]	Q_T/Q_M	Enhancement [%]
1	$T_{wm} = 120$ $T_m = 90$ $T_{wf} = 60$	404 508	0.632	—
2	$T_{wm} = 120$ $T_{m1} = 100$ $T_{m2} = 90$ $T_{m3} = 80$ $T_{wf} = 60$	489 753	0.765	21.1
3	$T_{wm} = 120$ $T_{m1} = 105$ $T_{m2} = 90$ $T_{m3} = 75$ $T_{wf} = 60$	493 178	0.771	21.9
4	$T_{wm} = 120$ $T_{m1} = 110$ $T_{m2} = 90$ $T_{m2} = 70$ $T_{wf} = 60$	466 976	0.730	15.4

From Table 3 the same observations can be obtained as those from Table 2. It is worth noting that the enhancement of the cumulative energy charged/discharged in each melting or freezing period is higher using 3 PCMs than 2 PCMs in a slab. In case 3 of this table, an enhancement of 21.9% can be obtained.

Figures 3 and 4 show the movement of the phase change interfaces corresponding to cases 3 in Tables 2 and 3, respectively. From Fig. 3 we can observe two phase change interfaces simultaneously progressing in the melting period and receding in the freezing period. Also, we can observe that the molten–frozen portion in each melting–freezing period at SRS is greater in the 2-PCM slab than in the single PCM slab. The same phenomena can be observed in Fig. 4. It should be indicated that the plateau in Fig. 4 is caused by the fixed grid method used in handling the latent heat effect. It is well known that this can be eliminated by mesh refinement.

Figure 5 displays a comparison of the dimensionless cumulative energy charged–discharged, Q_T/Q_M, vs the melting–freezing period among the single PCM slab,

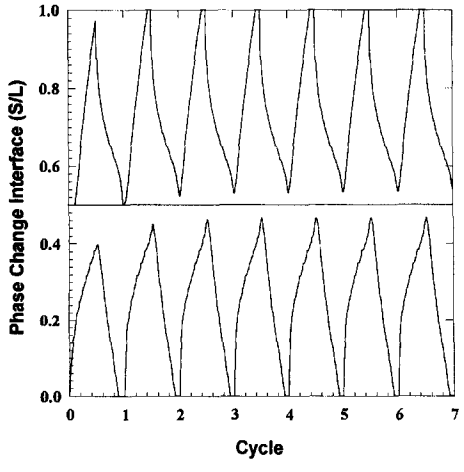

Fig. 3. Phase change interface movement vs time for 2-PCM slab (case 3 of Table 2).

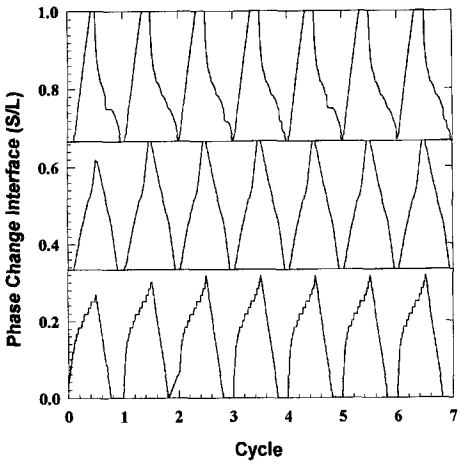

Fig. 4. Phase change interface movement vs time for 3-PCM slab (case 3 of Table 3).

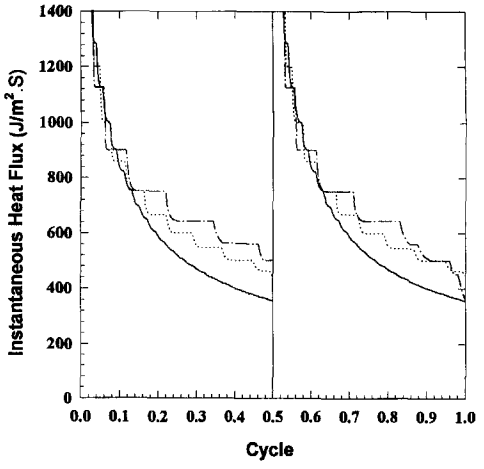

Fig. 6. Comparison of heat flux at the heat transfer surfaces.

case 3 in Table 2 for the 2-PCM slab and case 3 in Table 3 for the 3-PCM slab. The open circle line is for the single PCM, the open rectangle for the 2-PCM and the open triangle for the 3-PCM cases, respectively. In this figure, the discrete point values of Q_T/Q_M, each corresponding to either a melting period or a freezing period, are joined by line segments to show the trends of the process of energy charge–discharge. From this figure we can see the dynamic process from the initial condition to the SRS. For the single PCM slab, the oscillation of Q_T/Q_M disappears quickly; with continued cycling the alternative melting–freezing heat transfer process attains SRS after the second cycle. At SRS, the energy charged–discharged in the melting and the freezing period is identical. For the case of the 2-PCM slab, SRS is achieved after the third cycle and also the energy charged–discharged in a melting and a freezing period is the same at SRS. For the case of the 3-PCM slab, SRS is attained after cycle 8 (not displayed in this figure). At SRS the values of Q_T/Q_M are not exactly identical for each period. Q_T/Q_M oscillates slightly around an average value from cycle 8 to cycle 11 and afterwards, oscillates *ad infinitum* with a frequency of 3 Hz. Numerical experiments indicated that this slight oscillation is only observed in some (not all) composite PCM slabs and it is independent of mesh size.

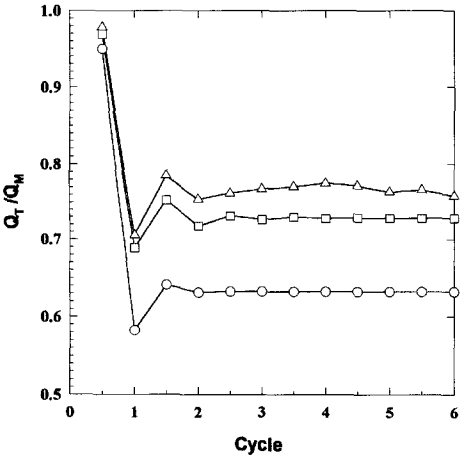

Fig. 5. Dimensionless cumulative energy charge–discharge vs melting–freezing periods.

Figure 6 demonstrates a comparison of the heat flux on the heat transfer surface in each melting and freezing period at SRS among the single PCM slab, case 3 in Table 2 for the 2-PCM slab and case 3 in Table 3 for the 3-PCM slab. The solid line is for the single PCM, the dotted line for the 2-PCM and the dash–dot line for the 3-PCM cases, respectively. At the earlier stage of each melting–freezing period the heat flux is a little lower in the 2-PCM slab than in the single PCM slab and in the 3-PCM slab than in the 2-PCM slab. After about one-fifth of a melting–freezing period, the heat flux begins to be higher in the 2-PCM slab than in the single PCM slab and in the 3-PCM slab than in the 2-PCM slab. From this figure we find that not only is the heat flux enhanced with multi-PCM slabs, but a uniform heat flux is attained in each melting or freezing period when more PCMs are used in a slab, especially in the last stage of the melting or freezing period. It should be noted that the step-like change of the heat flux is caused by the equivalent heat capacity method used. This is a weakness of equivalent heat capacity method in handling phase change effects. Every fixed grid method has the same kind of problem and this kind of problem can be alleviated by mesh refinement.

(2) *Effect of thermal conductivity ratio*

The same slab and boundary conditions as those of case 3 in Table 3 are used to investigate the effects of the thermal conductivity ratio on the enhancement of energy charge–discharge rates. The value of α_l/α_s is assumed to be 1.0 and held constant and all the other parameters are fixed except for changing the ratio of thermal conductivity k_l/k_s. Table 4 displays a comparison of the cumulative energy charged–discharged

Table 4. Effect of thermal conductivity ratio

[°C]	Case	k_l/k_s	$t_m = t_f$[s]		Q_T [J m^{-2}]	Q_T/Q_M	Enhancement [%]
$T_{wm} = 120$	1	1.0	650	single	404 508	0.632	
$T_m = 90$				3-PCM	493 178	0.771	21.9
$T_{wf} = 60$							
	2	0.4	1150	single	439 265	0.774	
$T_{wm} = 120$				3-PCM	534 425	0.941	21.7
$T_{m1} = 105$	3	0.2	1950	single	415 613	0.764	
$T_{m2} = 90$				3-PCM	517 257	0.969	26.9
$T_{m3} = 75$							
	4	0.1	3375	single	393 120	0.723	
$T_{wf} = 60$				3-PCM	517 790	0.955	31.7

Table 5. Effect of thermal diffusivity ratio

[°C]	Case	α_l/α_s	$t_m = t_f$ [s]		Q_T [J m^{-2}]	Q_T/Q_M	Enhancement [%]
$T_{wm} = 120$	1	1.0	650	single	404 508	0.632	
$T_{m1} = 105$				3-PCM	493 178	0.771	21.9
$T_{m2} = 90$							
	2	0.4	800	single	552 627	0.674	
$T_{m3} = 75$				3-PCM	627 102	0.765	13.5
$T_{wf} = 60$	3	0.2	1000	single	704 900	0.629	
				3-PCM	758 942	0.678	7.67

in each cycle at SRS. From this table we see that in the range of $k_l/k_s = 1.0 \sim 0.4$, the enhancements of the energy charge–discharge rates in each period are basically identical. Further decrease of the value of k_l/k_s can increase the enhancement of the energy charge–discharge rates. At $k_l/k_s = 0.1$, an enhancement of 31.7% can be expected.

(3) *Effect of thermal diffusivity ratio*

The same slab and boundary conditions as those of case 3 in Table 3 are utilised in this parametric investigation. The value of k_l/k_s is assumed to be 1.0 and held constant and all the other parameters are fixed except for changing thermal diffusivity ratio α_l/α_s. Table 5 gives a comparison of the cumulative energy charged/discharged in each period at SRS. From this table we can see that with the decrease of α_l/α_s the enhancement of the energy charge–discharge rates in each period decreases.

(4) *Effect of latent heat*

The same slab and boundary conditions as those of case 3 in Table 3 are used and all the parameters are the same as those used in case 3 of Table 3 and held constant except for changing the latent heat of the PCMs. Table 6 displays a comparison of the cumulative energy charged–discharged in each cycle at SRS. From this table we can see that with the increase of the latent heat of the PCMs, the enhancement of the energy charge–discharge rates increases.

(5) *Effects of the boundary conditions*

In this investigation, a 3-PCM slab is used and all the parameters used are the same as those used in case 3 of Table 3 except for the boundary temperatures (T_{wm} and T_{wf}) and the melting points of the PCMs. The computed cases and the results are listed in Table 7. From this table we can observe that the energy charge–discharge rate increases with decrease of the difference of the boundary melting and freezing temperatures. This is particularly favourable to low temperature applications since in low temperature applications the difference of retrieval temperature from the storage temperature is small.

CONCLUDING REMARKS

A finite element model was developed for alternate melting–freezing heat transfer in composite slabs consisting of several immiscible PCMs. Computations were carried out for cyclical melting–freezing in single and composite PCMs. The effects of different arrangements of melting points, thermophysical properties as well as boundary conditions on the energy charge–discharge process are investigated. Numerical experiments discovered that when a steady reproducible state is attained the charge–discharge rates of thermal energy can be significantly enhanced using composite PCMs with different melting points as compared with using a single PCM in a slab. As expected, magnitude of the enhancement depends on the arrangements of

Table 6. Effect of latent heat

[°C]	Case	λ	$t_m = t_f$[s]		Q_T[J m^{-2}]	Q_T/Q_M	Enhancement [%]
$T_{wm} = 120$	1	20 000	375	single	263 161	0.598	
$T_m = 90$				3-PCM	304 540	0.692	15.7
$T_{wf} = 60$							
	2	40 000	650	single	404 508	0.632	
$T_{wm} = 120$				3-PCM	493 178	0.771	21.9
$T_{m1} = 105$							
	3	80 000	1200	single	754 818	0.726	
$T_{m2} = 90$				3-PCM	945 164	0.909	25.2
$T_{m3} = 75$							
$T_{wf} = 60$							
	4	160 000	2150	single	1329 710	0.723	
				3-PCM	1756 840	0.955	32.1

Table 7. Effect of thermal swings

Case	$t_m = t_f$ [s]	[°C]	Q_T [J m^{-2}]	Q_T/Q_M	Enhancement [%]
		$T_{wm} = 80$			
		$T_m = 70$	363 228	0.757	
		$T_{wf} = 60$			
1	1750	$T_{wm} = 80$			
		$T_{m1} = 75$			
		$T_{m2} = 70$	457 240	0.953	25.9
		$T_{m3} = 65$			
		$T_{wf} = 60$			
		$T_{wm} = 120$			
		$T_m = 90$	404 508	0.632	
		$T_{wf} = 60$			
2	650	$T_{wm} = 120$			
		$T_{m1} = 105$			
		$T_{m2} = 90$	493 178	0.771	21.9
		$T_{m3} = 75$			
		$T_{wf} = 60$			
		$T_{wm} = 160$			
		$T_m = 110$	465 331	0.582	
		$T_{wf} = 60$			
3	400	$T_{wm} = 160$			
		$T_{m1} = 135$			
		$T_{m2} = 110$	545 623	0.682	17.3
		$T_{m3} = 85$			
		$T_{wf} = 60$			
		$T_{wm} = 200$			
		$T_m = 130$	579 027	0.603	
		$T_{wf} = 60$			
4	350	$T_{wm} = 200$			
		$T_{m1} = 165$			
		$T_{m2} = 130$	670 265	0.698	15.8
		$T_{m3} = 95$			
		$T_{wf} = 60$			

the PCMs, the thermophysical properties and the boundary conditions applied.

Acknowledgement—Z. X. Gong gratefully acknowledges the financial support of Canadian International Development Agency and McGill University in the form of a McGill/CIDA-Fellowship. Research support of Natural Science and Engineering Council of Canada as well as Exergex Corporation is also acknowledged.

REFERENCES

1. J. Bransier, Storage periodique par chaleur latente: aspects fonasmentaux\lies a la cinetique des transferts, *Int. J. Heat Mass Transfer* **22,** 875–883 (1979).
2. B. Kalhori and S. Ramadhyani, Studies on heat transfer from a vertical cylinder, with or without fins embedded in a solid phase change medium, *J. Heat Transfer* **107,** 44–51 (1985).
3. V. Jariwala, A. S. Mujumdar and M. E. Weber, The

periodic steady state for cyclic energy storage in paraffin wax, *Can. J. Chem. Engng* **65,** 899–906 (1987).
4. M. Hasan, Cyclic phase change: energy storage and recovery, Ph.D. Thesis, McGill University (1988).
5. K. Sasaguchi and R. Viskanta, Phase change heat transfer during melting and resolidification of melt around cylindrical heat source(s)/sink(s), *J. Energy Resour. Technol.* **111,** 43–49 (1989).
6. G. A. Adebiyi, A second-law study on packed bed energy storage systems utilizing phase-change materials, *J. Solar Energy Engng* **113,** 146–156 (1991).
7. C. Bellecci and M. Conti, Phase change thermal storage: transient behaviour analysis of a solar receiver/storage module using the enthalpy method, *Int. J. Heat Mass Transfer* **36,** 2157–2163 (1993).
8. C. Bellecci and M. Conti, Transient behaviour analysis of latent heat thermal storage module, *Int. J. Heat Mass Transfer* **36,** 3851–3857 (1993).
9. C. Bellecci and M. Conti, Latent heat thermal storage for solar dynamic power generation, *Solar Energy* **51,** 169–173 (1993).
10. T. W. Kerslake and M. B. Ibrahim, Analysis of thermal energy storage material with change of phase volumetric effects, *ASME J. Solar Energy Engng* **115,** 22–31 (1993).
11. Z. X. Gong Y. F. Zhang and A. S. Mujumdar, Cyclic phase change heat conduction in thin composite slabs. In *Computational Modelling of Free and Moving Boundary Problems* (Edited by L. C. Wrobel and C. A. Brebbia), Vol. 2, pp. 105–119. Computational Mechanics Publications (1991).
12. Z. X. Gong and A. S. Mujumdar, Cyclical heat conduction in melting and freezing of composite slabs of different phase change materials, *Proceedings of the 10th International Heat Transfer Conference*, Vol. 6, pp. 343–348 (1994).
13. M. M. Farid and A. Kanzawa, Thermal performance of a heat storage module using PCM's with different melting temperatures: mathematical modeling, *ASME J. Energy Resource Technol.* **111,** 152–157 (1989).
14. M. M. Farid, Y. Kim and A. Kanzawa, Thermal performance of a heat storage module using PCM's with different melting temperatures: experimental, *ASME J. Energy Resource Technol.* **112,** 125–131 (1990).
15. J. S. Lim, A. Bejan and J. H. Kim, Thermodynamic optimization of phase-change energy storage using two or more materials, *ASME J. Energy Resource Technol.* **114,** 84–90 (1992).
16. G. A. Adebiyi, B. K. Hodge, W. G. Steele, A. Jalaladeh and E. C. Nsofor, Computer simulation of a high temperature thermal energy storage system employing multiple family of phase-change storage materials, ASME-AES-Vol. 27/HTD-Vol. 228, pp. 1–11 (1992).
17. T. Watanabe, H. Kikuchi and A. Kanzawa, Enhancement of charging and discharging rates in a latent heat storage system by use of PCM with different melting temperatures, *Heat Recovery Systems CHP* **13,** 57–66 (1993).
18. Q. T. Pham, The use of lumped capacitance in the finite-element solution of heat conduction problems with phase change, *Int. J. Heat Mass Transfer* **29,** 285–291 (1986).
19. O. C. Zienkiewicz and R. L. Taylor, *The Finite Element Method.* McGraw-Hill, London (1989).
20. A. J. Dalhuijsen and A. Segal, Comparison of finite element techniques for solidification problems, *Int. J. Numer. Meth. Engng* **23,** 1807–1829 (1986).